frontiers | Frontiers in Earth Science

TYPE Original Research
PUBLISHED 14 May 2025
DOI 10.3389/feart.2025.1604873

OPEN ACCESS

EDITED BY
Mao-Wen Yuan,
China University of Geosciences, China

REVIEWED BY
Jie Li,
Hebei GEO University, China
Zhen Yan,
Chinese Academy of Geological Sciences (CAGS), China
Chuan Xu,
Chengdu University of Technology, China

*CORRESPONDENCE
Jian Guo,
guojian9818@163.com

RECEIVED 02 April 2025
ACCEPTED 28 April 2025
PUBLISHED 14 May 2025

CITATION
Guo J, Li Z, Nie J, He S, Wang J and Khan W (2025) Uranium-polymetallic mineralization relationship and comprehensive mineralization model in the Xiangshan ore field, South China: constraints from H-O-S-Pb-Sr multi-isotope data. *Front. Earth Sci.* 13:1604873. doi: 10.3389/feart.2025.1604873

Uranium-polymetallic mineralization relationship and comprehensive mineralization model in the Xiangshan ore field, South China: constraints from H-O-S-Pb-Sr multi-isotope data

Jian Guo[1,2,3]*, Ziying Li[1,2,3], Jiangtao Nie[1,2,3], Sheng He[1,2,3], Junxian Wang[1,2,3] and Waseem Khan[2]

[1]National Key Laboratory of Uranium Resource Exploration-Mining and Nuclear Remote Sensing, Beijing, China, [2]Beijing Research Institute of Uranium Geology, Beijing, China, [3]CNNC Key Laboratory of Uranium Resource Exploration and Evaluation Techniques, Beijing, China

The Xiangshan ore field, recognized as China's premier volcanic-hosted uranium deposit cluster, has recently revealed significant exploration breakthroughs through the discovery of vertically zoned Pb-Zn-Ag-Cu polymetallic mineralization beneath shallow uranium systems, establishing a characteristic "upper uranium-lower polymetallic" vertical zoning configuration. This distinctive metallogenic architecture has propelled investigations into the genetic connections and superimposed mineralization mechanisms between deep polymetallic systems and surficial uranium enrichment, representing a pivotal frontier for advancing comprehensive evaluation strategies of uranium-polymetallic resources in volcanic terrains. Through systematic comparative analysis of H-O-S-Pb-Sr isotopic signatures across both mineralization types, this study elucidates: (1) Uranium mineralization exhibits significantly higher meteoric water contributions ($\delta^{18}O_{H2O}$: 0.95‰–4.95‰) and crustal material inputs ($^{87}Sr/^{86}Sr$: 0.71447 to 0.72072; $\delta^{34}S$: 6.2‰–19.55‰) compared to polymetallic counterparts; (2) $^{206}Pb/^{204}Pb$, $^{207}Pb/^{204}Pb$, and $^{208}Pb/^{204}Pb$ ratios for sulfide minerals of polymetallic mineralization ranging from 17.599 to 18.262, 15.558 to 15.725, and 37.934 to 38.875 and sample points exhibit a linear distribution pattern imply unique sulfur enrichment processes potentially associated with uranium-rich hydrothermal systems; (3) Multivariate isotopic evidence confirms that uranium and polymetallic mineralization represent products of two discrete metallogenic events under the extensional tectonic regime of South China.

KEYWORDS

Xiangshan ore field, uranium mineralization, polymetallic mineralization, multi-isotope data, metallogenic model

1 Introduction

The Xiangshan orefield, located in Fuzhou, Jiangxi province, is a typical representative of volcanic-type uranium deposit in China and has been investigated for about 60 years (Guo et al., 2020; Li and Zhang, 2016). Within a range of 300 square kilometers, over 30 uranium deposits/occurrences were discovered, and most of them were kept above the depth of 500 m. At long-term exploration and study, geologists have accumulated many sources about structural evolution (e.g., Li et al., 2014), magmatism (e.g., Guo et al., 2016), ore-forming fluid (e.g., Fan et al., 2003) and metallogenic age (e.g., Liu et al., 2015). In the recent decade, a lot of polymetallic mineralization under the uranium ore (700 m–2,000 m), discovered by deep drilling, has attached wide attention as a new focus of metallogenic research. So far, studies on polymetallic mineralization is just on the ascent, and several studies in Chinese refers to the mineralogy, metallogenic characteristics, fluid inclusion, and ore genesis (Guo et al., 2018; Wang et al., 2014a; Wu and Hu, 2014; Nie et al., 2015; Wang et al., 2015). Relatively systematic comparative research on uranium and polymetallic mineralization has not yet been extensively conducted, particularly lacking isotopic composition comparisons that are crucial for revealing the sources of ore-forming materials and metallogenic mechanisms. The recently implemented China Uranium Scientific Drilling (Abbrev. CUSD1) has revealed uranium and polymetallic deposits within the same borehole, exhibiting a vertical spatial distribution pattern of "uranium above and polymetals below." This borehole provides an ideal section for systematically collecting samples and conducting in-depth comparative studies.

In this paper, we describe the metallogenic geological characteristics of the uranium-polymetallic mineralization and report H-O-S-Pb-Sr isotopic data and whole-rock Pb and Rb-Sr isotope of the wall rock. These new datasets, together with preciously published results, are utilized to constrain the sources of ore-forming fluids and metals and metallogenic mechanism. Based on previous research findings, this study investigated the magmatic and metallogenic epochs of the Xiangshan ore field, and established a uranium-polymetallic metallogenic model under regional extensional setting. Meanwhile, we take an in-depth comparison between uranium and polymetallic mineralization and establish a comprehensive ore-forming model for uranium-polymetallic mineralization.

2 Geological background

2.1 Regional geology and local geology

The Xiangshan uranium ore field is structurally situated within a large-scale volcanic collapse basin. This volcanic-intrusive basin, located in the Cretaceous extensional tectonic zone between the Yangtze and Cathaysia blocks (Li et al., 2014), occupies a critical metallogenic position in southeastern China. Specifically, it is positioned at the southwestern margin of the Gan-Hang tectonic belt and the northeastern periphery of the Qin-Hang metallogenic belt (Figure 1), where it developed through intense magmatic-tectonic interactions during the Late Mesozoic continental extension.

The basement of the volcanic basin consists mainly of low greenschist facies to low amphibolite facies Paleo-Mesoproterozoic metamorphic rocks (amphibolite and schist) and the less-metamorphosed Neoproterozoic (Sinian system) rocks, including phyllite, slate, and metasandstone (Yang et al., 2010). The volcanic rocks from the Xiangshan include rhyolitic crystal tuffs, welded tuffs, rhyodacites, porphyroclastic rhyolite, associated subvolcanic rocks such as monzogranite-porphyry and granite-porphyry, and late dykes such as quartz monzonitic porphyry and lamprophyre. Previous studies showed that the volcanic cover was formed by two cycles (Figure 2). The first volcanic cycle represents a fissure eruption and is composed mainly of rhyodacite that yielded a zircon U-Pb age of 135 Ma (Li et al., 2014; Yang et al., 2010) and rhyolitic welded tuff. The second volcanic cycle was a central vent eruption and was composed mainly of extrusive facies of felsic lava that formed the main part of the Xiangshan volcanic-intrusive complex, yeilding a zircon U-Pb age of 132 Ma (Li et al., 2014).

So far, almost 30 uranium deposits have been discovered, mainly distributed in the western and northern Xiangshan. Uranium mineralization occurs in fractures attached to NE-trending faults, which cut the volcanic-intrusive complex without dependence on wall rock. Polymetallic mineralization has been discovered at depths of 500–1,500 m below uranium ore bodies, such as in the Niutoushan area (boreholes ZK26-9, ZK26-11, ZK26-101), the Heyuanbei area (CUSD3), and the Niuonaoshang area (CUSD1). The mineralization occurs in both overlying volcanic rocks and basement metamorphic rocks, showing no selectivity toward host rocks. Spatially, the two mineralization types (uranium and polymetallic) exhibit a vertical zoning characterized by "uranium above and polymetallic below" (Figure 3).

2.2 Geology of uranium and polymetallic mineralization

The CUSD1 has been carried out in the Xiangshan volcanic basin, 2 km southeast of the Zoujiashan uranium deposit, with a final depth of 2818 m for the main hole. Three uranium mineralizations and five polymetallic mineralizations, with hydrothermal alteration developing, have been recovered by CUSD1.

Uranium mineralization occurs in cataclastic rhyolite at shallow depths of 200–900 m in borehole CUSD1, with strongly developed hydrothermal alteration such as albitization, hematitization (Figure 4a), fluoritization, carbonatization (Figure 4b), and pyritization. The ore exhibits vein-type and stockwork-type mineralization. The main ore minerals are pitchblende (Figure 4c), brannerite, conffinite, thorite, pyrite, minor molybdenite, chalcopyrite, galena, sphalerite, and native bismuth. The main gangue minerals are calcite, fluorite, quartz, apatite, minor rutile and monazite.

Polymetallic mineralization occurs within the deep-seated basement metamorphic rocks at vertical depth of 1,400–2,800 m in borehole CUSD1, primarily characterized by hydrothermal alterations such as silicification (Figure 4d), carbonatization, sericitization, and chloritization. The main ore minerals are galena, sphalerite (Figure 4f), arsenopyrite (Figure 4e), pyrite, pyrrhotite, minor chalcopyrite, and argentite. The main gangue minerals are quartz, calcite, siderite, minor sericite, chlorite, and cassiterite.

10.3389/feart.2025.1604873

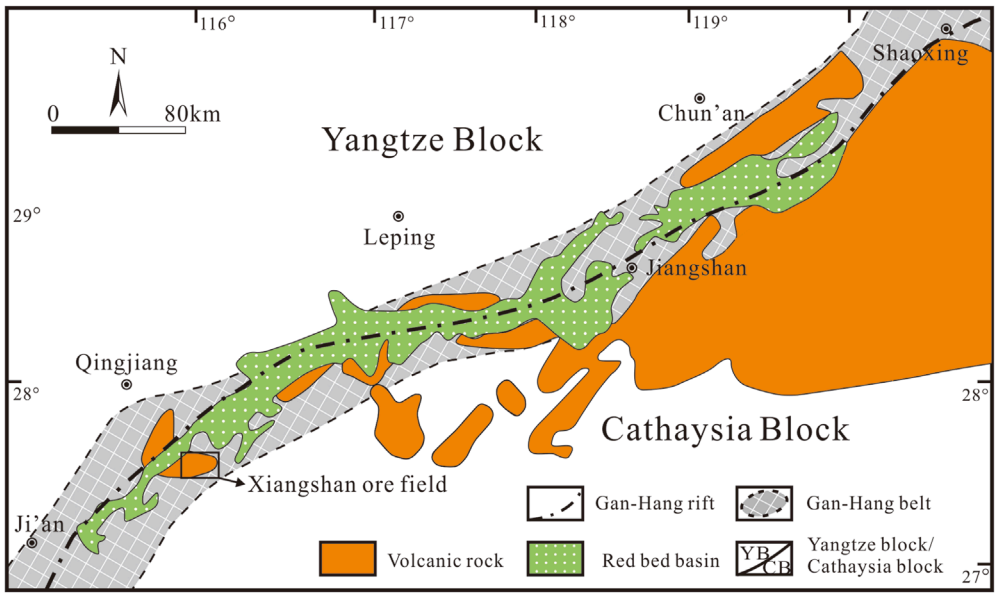

FIGURE 1
Geological sketch map showing the Gan-Hang Belt. Modified after Yu et al. (2006).

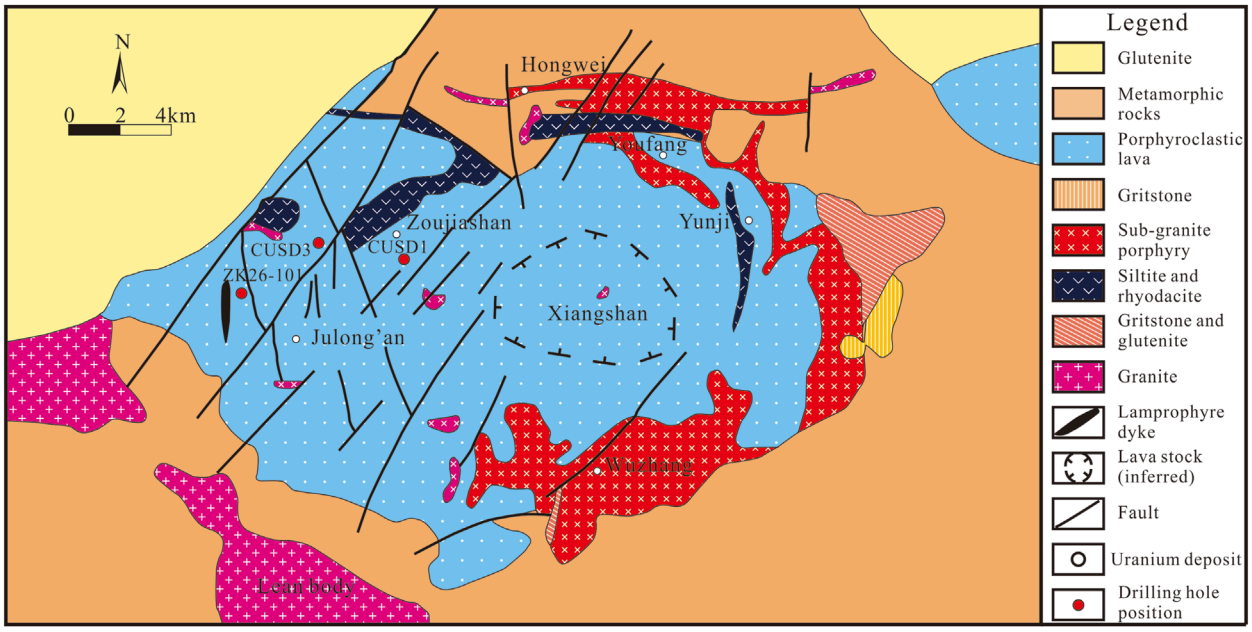

FIGURE 2
Geological map of Xiangshan volcanic-intrusive complex. Modified after Li and Zhang (2016) and Guo et al. (2020).

10.3389/feart.2025.1604873

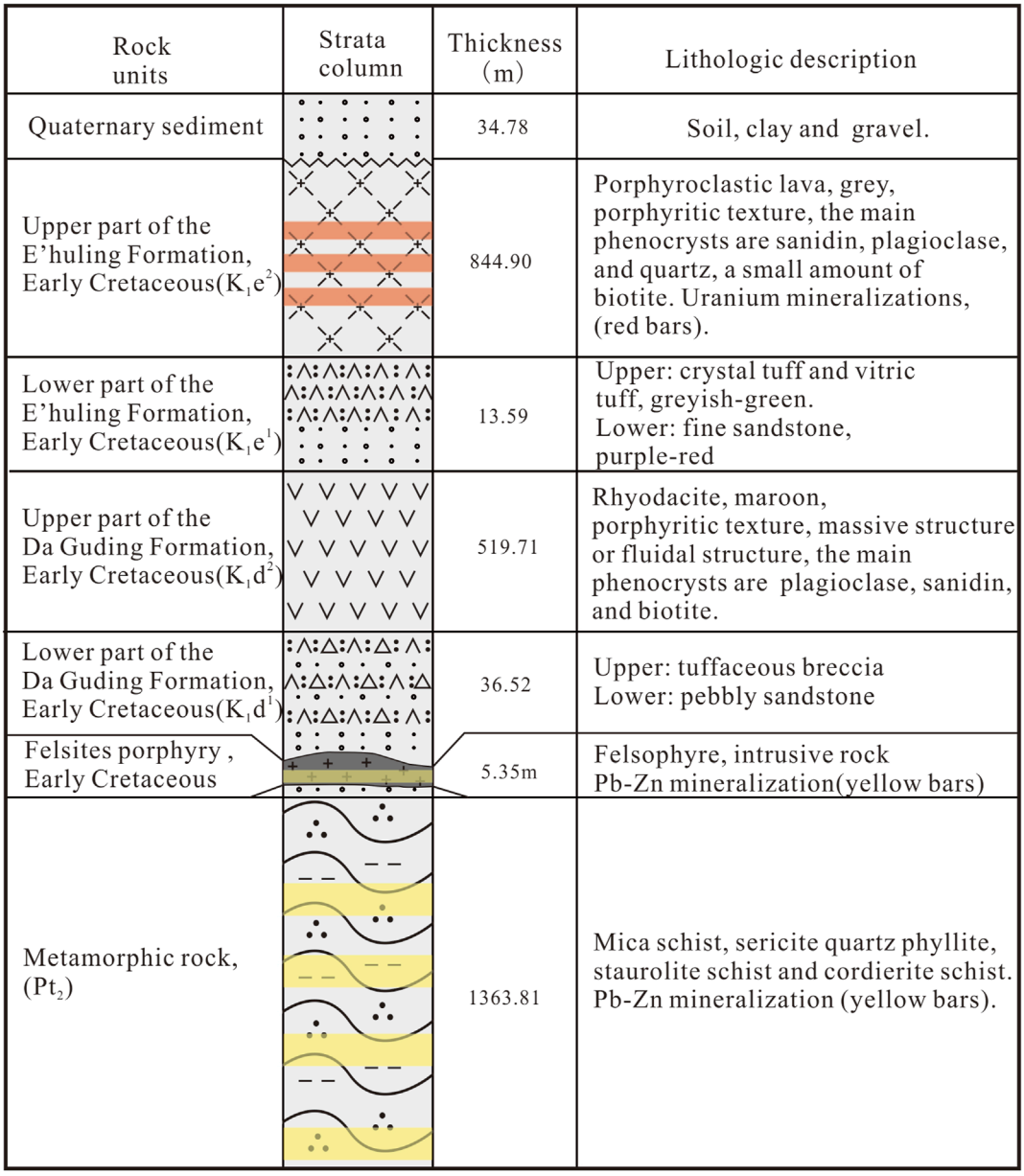

FIGURE 3
The stratigraphic column of the CUSD1. Total drilling depth is 2818 m.

3 Samples and analytical methods

3.1 Sampling

All samples used in this study were collected from CUSD1, including monomineralic samples for multi-isotope analysis and fresh rock samples. Mineral separates were extracted from crushed and washed sample fragments (40–60 mesh) and were handpicked under a binocular microscope to achieve a purity of >99%. Each grain was carefully examined in order to avoid inclusions.

3.2 Analytical methods

H-O-S-Pb-Sr isotope analyses were performed in the Analytical Laboratory of the Beijing Research Institute of Uranium Geology.

The H-O isotope analysis of calcite and quartz single minerals was conducted using a MAT253 isotope mass spectrometer. The $\delta^{18}O$ measurement was obtained by generating O_2 using the BrF_5 method, which was then converted to CO_2 for analysis on the mass spectrometer to obtain the hydrogen and oxygen isotope composition. Through standard calculations, the ΔD_{H2O} of the inclusions was obtained, with an analytical precision of ±2%.

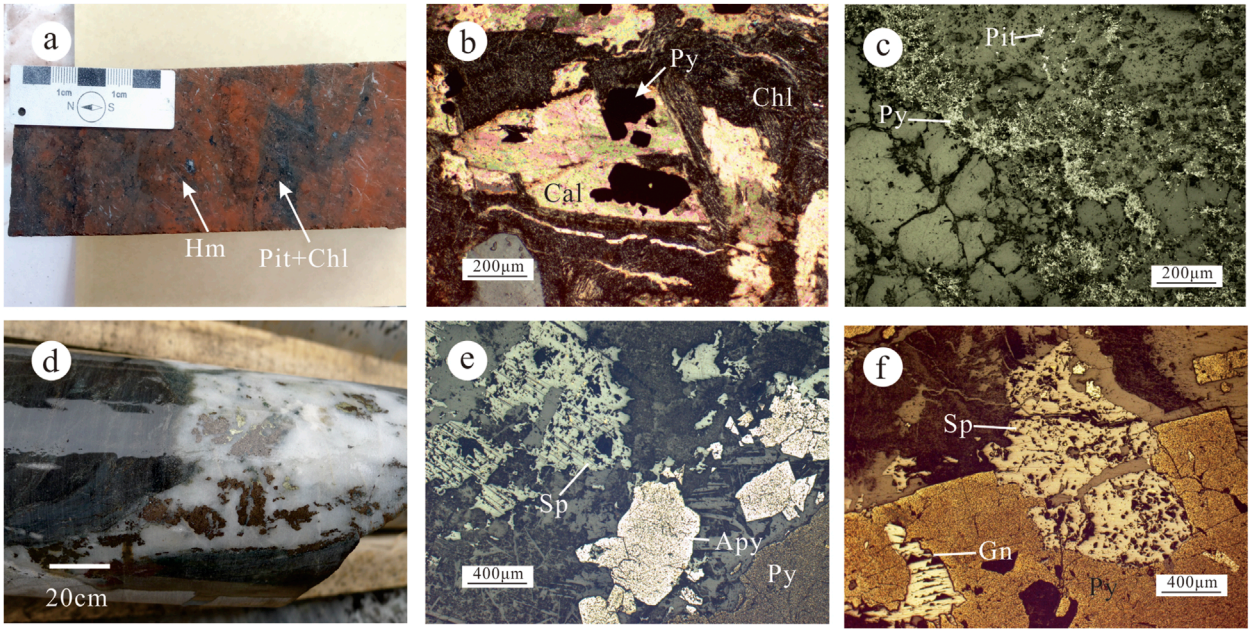

FIGURE 4
Microscopic characteristics of uranium and polymetallic mineralization in the Xiangshan Uranium Ore Field. **(a)** Strongly hematitized uranium ore; **(b)** Intense carbonatization and chloritization; **(c)** Disseminated pyrite-pitchblende assemblage; **(d)** Banded polymetallic ore; **(e)** Paragenesis of sphalerite, arsenopyrite, and pyrite; **(f)** Sphalerite and galena replacing pyrite, displaying replacement relict texture. Abbreviations: Hm- Hematite, Cal - Calcit e, Chl - Chlorite, Pit - Pitchblende, Py - Pyrite, Sp - Sphalerite, Gn - Galena, Apy - Arsenopyrite.

The sulfur isotope compositions of sulfide samples were analyzed on a MAT251E gas mass spectrometer by using Cu_2O to oxidize the sulfides. The analytical procedure usually yielded an in-run precision of 0.2‰. The calibration were performed with regular analyses of internal $\delta^{34}S$ standard samples.

The lead isotope compositions of sulfide samples were analyzed on the GV IsoProbe-T Thermal Ionization Mass Spectrometer. The analytical procedure involved dissolution of samples using HF and $HClO_4$ in crucibles, followed by basic anion exchange resin to purify Pb. Analytical results for the standard NBS 981 are $^{208}Pb/^{204}Pb$ = 36.611 ± 0.004 (2σ), $^{207}Pb/^{204}Pb$ = 15.457 ± 0.002 (2σ), and $^{206}Pb/^{204}Pb$ = 16.937 ± 0.002 (2σ), in agreement with the reference value (Belshaw et al., 1998).

The strontium isotope composition was determined on a multicollector IsoProbe-T Thermal Ionization Mass Spectrometer. Details of the chemical separation and mass spectrometric procedures are described by Wang et al. (2014b). $^{87}Sr/^{86}Sr$ is normalized to $^{88}Sr/^{86}Sr$ = 8.375219 to correct for instrumental fraction. During the period of this study, measurement for the American Standard Reference Material NBS 987 Sr standard gave $^{87}Sr/^{86}Sr$ = 0.710250 ± 0.000007 (2σ). The total procedural blanks for Rb and Sr were 0.2 ng and 0.2 ng, respectively.

4 Analytical results

4.1 H-O isotope

The analytical results of hydrogen and oxygen isotopes for uranium-polymetallic mineralization are presented in Table 1. The $\delta^{18}O_{H2O}$ values were obtained based on the modal temperature measurements of fluid inclusions and the oxygen isotope equilibrium fractionation formulas for the SiO_2-H_2O and $CaCO_3$-H_2O systems. During the uranium mineralization period, the $\delta^{18}O$ values of four calcite samples ranged from 8.6‰ to 12.6‰, with an average of 10.63‰. The calculated $\delta^{18}O_{H2O}$ values ranged from 0.95‰ to 4.95‰, averaging 2.98‰, while the $\delta^{18}D$ values ranged from −87.3‰ to −78.1‰. During the polymetallic mineralization period, the $\delta^{18}O$ values of ten quartz samples ranged from 10.4‰ to 14.7‰, with an average of 13.7‰. The calculated $\delta^{18}O_{H2O}$ values ranged from 3.51‰ to 7.81‰, averaging 6.80‰, while the $\delta^{18}D$ values ranged from −91.3‰ to −71.4‰.

4.2 Sulfur isotope

S isotope compositions of pyrite, pyrrhotite, sphalerite, and arsenopyrite separated from the polymetallic mineralization of CUSD1, together with previously published data (Nie et al., 2015), are listed in Table 2 and showed in histogram (Figure 5). Fourty-five $\delta^{34}S$ values of sulfides range from 2 to 6.9‰, with an average value of 4.16‰. The sulfur isotope compositions of pyrite, pyrrhotite, sphalerite, and arsenopyrite range from 2.2‰ to 6.9‰ (n = 21), from 2 to 5.8‰ (n = 12), from 3.3‰ to 3.9‰ (n = 4), and from 3.1 to 4.8 (n = 6), respectively. The obtained single sulfur isotope values of galena and chalcopyrite from polymetallic mineralization are 2.5‰ and 4.6‰. The S isotope compositions of pyrite in uranium mineralization differ significantly from those of galena and chalcopyrite. The S isotope values of 24 pyrites show strong $\delta^{34}S$ enrichment, with a wide distribution range and values of $\delta^{34}S$

TABLE 1 H-O isotope composition of uranium and polymetallic mineralization.

Type of mineralization	Sample number	Sample location/Depth	Sample type	$\delta^{18}O_{Minerals}$‰	$\delta^{18}O_{H2O}$‰[b]	δD‰	Tempreture (°C)[a]	Data source
Uranium mineralization	V057	Zoujiashan deposit	Calcite	12.2	4.55	−78.1	240	This study
	V090	Zoujiashan deposit	Calcite	12.6	4.95	−79.6	240	
	V177	Zoujiashan deposit	Calcite	8.6	0.95	−87.3	240	
	V178	Zoujiashan deposit	Calcite	9.1	1.45	−85.9	240	
Polymetallic mineralization	B598-1	CUSD1 (1795.5 m)	Quartz	10.4	3.51	−81.4	300	This study
	B643-1	CUSD1 (1929.3 m)	Quartz	14.1	7.21	−78.7	300	
	B660-2	CUSD1 (1980.6 m)	Quartz	14.0	7.11	−89.9	300	
	B672-1	CUSD1 (2016.1 m)	Quartz	14.2	7.31	−91.3	300	
	B756-3	CUSD1 (2268.8 m)	Quartz	14.1	7.21	−77.3	300	
	B760-1	CUSD1 (2280.1 m)	Quartz	12.4	5.51	−76.7	300	
	B788-1	CUSD1 (2364.2 m)	Quartz	14.4	7.51	−73.6	300	
	B795-2	CUSD1 (2385.8 m)	Quartz	14.3	7.41	−80.7	300	
	D070	CUSD1 (2428.6 m)	Quartz	14.7	7.81	−77.9	300	
	D080	CUSD1 (2705.3 m)	Quartz	14.3	7.41	−71.4	300	

Remarks:

[a]Average microthermometric value of fluid inclusions in uranium and polymetallic mineralization.

[b]Caculation result,The calculation formula is as follows:

$\delta^{18}O_{water} = \delta^{18}O_{mineral} - 1000 \ln \alpha_{mineral-water}$

$\delta^{18}O_{quatz} - \delta^{18}O_{water} = 1000 \ln \alpha_{quartz-water} = 3.38 \times 10^6/T^2 - 3.40$[12]

$\delta^{18}O_{calcite} - \delta^{18}O_{water} = 1000 \ln \alpha_{calcite-water} = 2.78 \times 10^6/T^2 - 2.89$[13]

10.3389/feart.2025.1604873

TABLE 2 S isotope composition of uranium and polymetallic mineralization in Xiangshan ore-field.

Sample type	Sample location/Depth	Mineral	$\delta^{34}S$/‰	Average	Sample quantity	Data source
Uranium mineralization	Shazhou deposit	Pyrite	9.6–19.55	14.65	15	Yan et al. (2013)
	Shazhou deposit	Pyrite	6.2–15.0	10.93	8	Si (2018)
	Shazhou and Hengjian deposits	Pyrite	7.9–14.9	12.35	6	Wu and Hu (2014)
Polymetallic mineralization	CUSD1	Pyrite, Pyrrhotite and Arsenopyrite	2–6.9	4.32	24	This study
	CUSD1	Pyrite, Pyrrhotite, Sphalerite and galena	2.6–6.6	3.99	21	Nie et al. (2015)

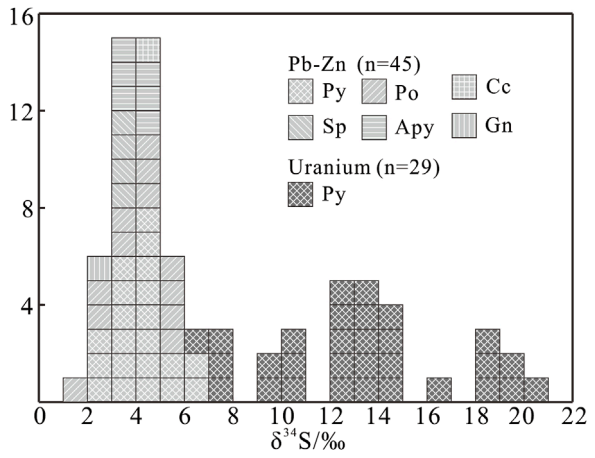

FIGURE 5
Histogram of sulfur isotope composition of uranium and polymetallic mineralization.

between 6.2‰ and 19.55‰. The average $\delta^{34}S$ value of pyrite in uranium ore is 13.15‰.

4.3 Lead isotope

Pb isotope compositions of polymetallic mineralization, uranium ore, porphyroclastic rhyolite, rhyodacite, and metamorphic basement are listed in Table 3, respectively. We estimate the Pb isotope compositions of metamorphic basement with U, Th, and Pb values, denoting an age of 130 Ma, which is the sulfide Rb-Sr dating age (Yang et al., 2015; Guo et al., 2018), to exclude the influence of radioactive lead. We use the Pb isotope compositions of volcanic rock, porphyroclastic rhyolite, and rhyodacite without estimating because of the same age between polymetallic mineralization and the formation of volcanic rock.

$^{206}Pb/^{204}Pb$, $^{207}Pb/^{204}Pb$, and $^{208}Pb/^{204}Pb$ ratios for sulfide minerals of polymetallic mineralization ranging from 17.599 to 18.262, 15.558 to 15.725, and 37.934 to 38.875; for pyrite from uranium ore ranging from 18.221 to 19.372, 15.591 to 15.717, and 38.504 to 38.910; for volcanic rock ranging from 18.471 to 18.792, 15.618 to 15.652, and 38.634 to 39.182. The estimated ratios of metamorphic basement range from 17.968 to 18.623, 15.553 to 15.633, and 38.304 to 38.753.

Sulfide samples have relatively homogeneous and characteristically low radiogenic lead; those from uranium ore is more radiogenic than sulfide from polymetallic mineralization.

4.4 Strontium isotope

The Sr isotope compositions of uranium mineralization, polymetallic mineralization, and major geological units in the Xiangshan ore field were obtained (Table 4). The analyzed results indicate that the Sr isotope composition of cataclastic rhyolite ranges from 0.710511 to 0.713861, with an average of 0.712225. The Sr isotope composition of rhyodacite ranges from 0.710773 to 0.711841, averaging at 0.711147. The Sr isotope composition of the basement metamorphic rocks ranges from 0.718085 to 0.724013, averaging at 0.720212, which is significantly higher than that of the volcanic rocks. The Sr isotope composition of individual fluorite minerals in uranium mineralization ranges from 0.71447 to 0.72072, averaging at 0.71752 (Jiang et al., 2006). The Sr isotope composition of individual pyrite minerals in polymetallic mineralization ranges from 0.719656 to 0.720133, averaging at 0.719833, which is higher than that of individual fluorite minerals in uranium mineralization and similar to the whole-rock Sr isotope composition of the basement metamorphic rocks.

5 Discussion

5.1 Multivariate isotope composition and comparison

5.1.1 H-O isotope

The H-O isotope composition results of the ore-forming fluids in the polymetallic mineralization mainly fall within the range of magmatic water (Figure 6). The hydrogen and oxygen isotope composition results of uranium mineralization are relatively close to those of magmatic water but show a slight deviation toward

TABLE 3 Statistical results of the Pb isotope compositions of the uranium mineralization, polymetallic mineralization, volcanic rocks and metamorphic basement.

Sample type	Sample quantity	$(^{206}Pb/^{204}Pb)_{131Ma}$		$(^{207}Pb/^{204}Pb)_{131Ma}$		$(^{208}Pb/^{204}Pb)_{131Ma}$		Data source
		Range	Average	Range	Average	Range	Average	
Uranium mineralization	11	18.221–19.372	18.430	15.591–15.717	15.644	38.504–38.910	38.671	Yang et al., 2015; Sun et al., 2004
Polymetallic mineralization	15	17.599–18.262	18.176	15.558–15.725	15.634	37.934–38.875	38.600	This study
Rhyolite	21	18.476–18.758	18.553	15.618–15.652	15.630	38.634–39.047	38.908	This study
Rhyodacite	14	18.471–18.792	18.625	15.630–15.650	15.638	38.768–39.182	38.945	This study
Metamorphic rock	10	17.968–18.623	18.212	15.553–15.633	15.592	38.304–38.753	38.435	This study

the meteoric water line. This evidence suggests that the isotopic composition of uranium ore-forming fluids is similar to that of polymetallic mineralization, with both primarily derived from magmatic water. However, the uranium ore-forming fluids exhibit a higher contribution of meteoric water compared to the polymetallic mineralization.

5.1.2 Sulfur isotope composition

Primary ores from the polymetallic mineralization are composed chiefly of pyrite, pyrrhotite, galena, sphalerite, and arsenopyrite. The lack of sulfate minerals in ores suggests that $\delta^{34}S$ value of the hydrothermal fluid can be represented by that of sulfide minerals. All ore minerals have $\delta^{34}S$ values that are relatively high, with a range of 2–6.9‰ (average 4.16‰). These values are close to the meteorite and meomantle-derived magmatic sulfur (0‰ ± 3‰, Rollinsion, 1993), suggesting a deep crust and upper mantle source (Wang et al., 2014b).

The sulfur isotope composition of pyrite during the uranium mineralization period ranges from 9.6‰ to 19.55‰, with an average of 14.65‰ and a range (difference between the maximum and minimum values) of 9.95‰. This composition is significantly higher than that of the main stratigraphic units and polymetallic mineralization in the Xiangshan ore field (Figure 7), and the range of isotope composition is relatively large. Previous studies have shown that the uranium ore-forming materials in the Xiangshan ore field mainly originated from deep-sourced magma (Li et al., 2014; Guo, 2014). The isotope composition ranging from 9.6‰ to 19.55‰ and the large range indicate that, compared to polymetallic mineralization, the uranium mineralization period involved a greater contribution of crustal sulfur.

5.1.3 Lead isotope composition

Generally, if lead from different geological units is derived from the same source, the Pb isotope compositions and variation trends should be similar (Cannon et al., 1961). The isotopic values from the volcanic rock and metamorphic basement were compared to the Pb isotopic compositions of sulfides from the polymetallic mineralization. The Pb isotopic composition of the ores mostly falls in the metamorphic basement-forming region, which is very far from the volcanic rock-forming region (Figure 8). The volcanic rock is dated at ca. 132 to 135 Ma (Guo, 2014; Li et al., 2014), which closely matches the age of the polymetallic mineralization (131 Ma, Liu et al., 2019). However, the Pb isotope composition of the volcanic rock is inconsistent with that of the polymetallic ore, which also suggests that it could not have been a significant source of lead in the ores. Considering that the ore sufides were the result of fluid-rock interaction, the metamorphic basement is possibly a major source for lead and other metals in the Pb-Zn mineralization (Guo et al., 2018).

Compared to polymetallic sulfides, the lead isotope composition of pyrite in uranium ores is relatively closer to the distribution range of lead isotopes in metamorphic rock bases and orogenic belts (Figure 8). This suggests that more components from surrounding rocks such as the basement and volcanic rocks were incorporated during uranium mineralization. The sample points in the polymetallic mineralized sulfides also exhibit a linear distribution pattern. Compared to most samples, there is an addition of radiogenic lead in the sulfides, and the distribution pattern of lead isotope composition is similar to that of pyrite samples from uranium mineralization. This indicates that during the process of polymetallic mineralization, there may have been a relative enrichment of uranium due to the polymetallic mineralization process.

5.1.4 Strontium isotope composition

Based on the age of polymetallic mineralization in Xiangshan area (about 131 Ma), we calculated the initial Sr isotope compositions of the sulfide and whole-rock. Sulfide separates from the polymetallic mineralization has initial $^{87}Sr/^{86}Sr$ ratios ranging from 0.719656 to 0.720133, which is higher than that of the continental crust mean value of 0.719 (Zeng et al., 2020).

10.3389/feart.2025.1604873

TABLE 4 Sr isotope composition of uranium mineralization, polymetallic mineralization, and various geological units in the Xiangshan area.

Samples	Rb ($\times10^{-6}$)	Sr ($\times10^{-6}$)	$^{87}Rb/^{86}Sr$	$^{87}Sr/^{86}Sr$	$(^{87}Sr/^{86}Sr)_t$	Data source
Rhyolite						This study
B1-1	248	168	4.2858	0.718491	0.710511	
B031	282	80.6	10.1231	0.730900	0.712051	
B285-1	280	80.1	10.1221	0.732708	0.713861	
B252-6	277	62.5	12.845	0.736394	0.712477	
Rhyodacite						This study
B145	287	227	3.6657	0.717598	0.710773	
B151	308	250	3.5598	0.718469	0.711841	
B407-1	322	194	4.8056	0.719389	0.710441	
B465-1	321	229	4.0540	0.719079	0.711531	
Metamorphic rock						This study
B480	146	266	1.5907	0.721047	0.718085	
B506-1	162	98.5	4.7672	0.732889	0.724013	
B615-1	179	291	1.7765	0.723221	0.719913	
B804-1	156	216	2.0933	0.722736	0.718838	
Polymetallic mineralization						This study
GJ-1–3	4.27	9.88	1.2506	0.722165	0.719836	
GJ-1–4	25.2	39.4	1.8496	0.723137	0.719693	
GJ-2–3	4.31	10.1	1.2352	0.722128	0.719828	
GJ-4–2	26.9	18.9	4.1087	0.727501	0.719851	
GJ-4–3	7.38	15.4	1.3886	0.722241	0.719656	
GJ-3–3	4.27	12.0	1.0248	0.722041	0.720133	
Uranium mineralization						Jiang et al. (2006)
XS9-1	22.22	295.4	0.218	0.721028	0.72072	
XS9-11	4.3	440.9	0.028	0.719703	0.71966	
XZ9-21	8.55	1136.0	0.022	0.714502	0.71447	
XZ9-26	70.82	741.9	0.277	0.715615	0.71523	

The metamorphic rock has $(^{87}Sr/^{86}Sr)$ t (t = 131 Ma) ratios ranging from 0.718085 to 0.724013 (Table 3), including the $^{87}Sr/^{86}Sr$ ratios range of sulfides. The volcanic rocks, including rhyolite and rhyodacite, have $(^{87}Sr/^{86}Sr)$ t (t = 131 Ma) ratios ranging from 0.7103 to 0.7139 (Table 3), lower than those of sulfides and lower metamorphic basement. Therefore, the source materials for the polymetallic mineralization may have been derived mainly from the crust repository, most likely come from the metamorphic basement.

Compared to polymetallic mineralization, uranium mineralization exhibits a broader range of strontium isotope compositions, displaying a bimodal characteristic (Figure 9).

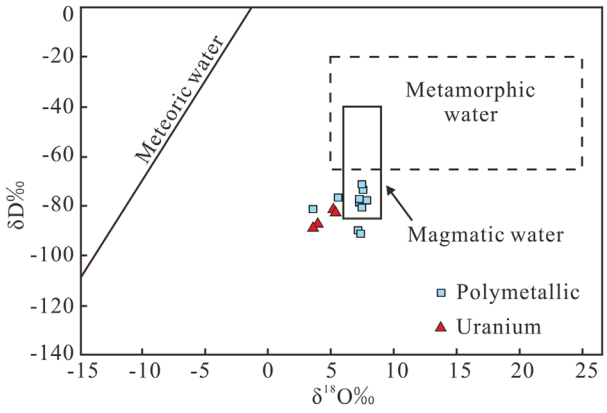

FIGURE 6
H-O isotopes composition of uranium and polymetallic mineralization (modified after Taylor, 1979).

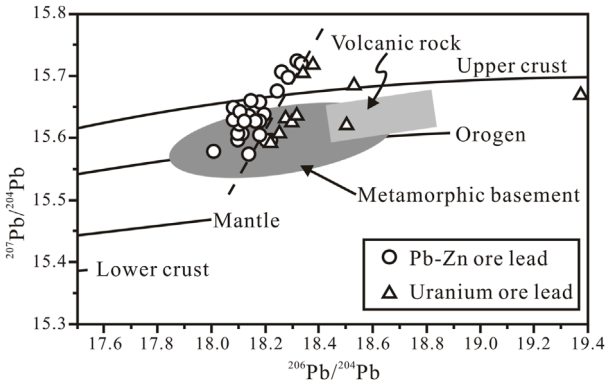

FIGURE 8
Uranium-polymetallic mineralization and lead isotope composition of major geological units in the Xiangshan ore field. Trends for the upper crust, orogen, mantle, and lower crust are taken from Zartman and Doe (1981).

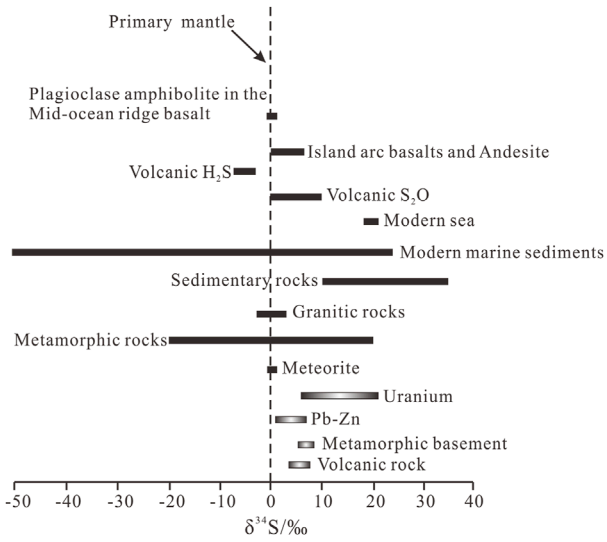

FIGURE 7
Uranium polymetallic mineralization and sulfur isotope composition of major geological units in the Xiangshan ore field. The sulfur isotope composition of main geological unit come from Kelly and Rye, 1979, Chaussidon and Lorand, 1990, and Rollinson 2014.

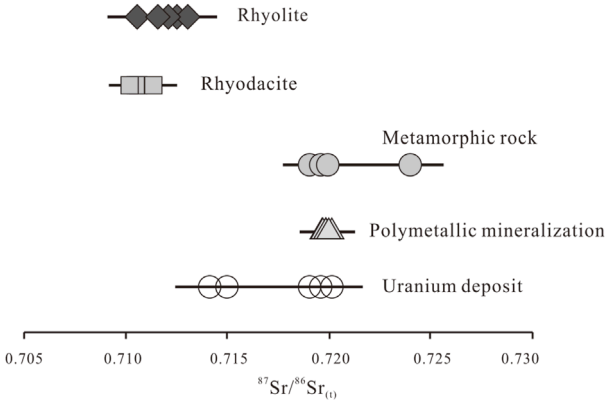

FIGURE 9
Comparison of initial Sr isotope values between uranium mineralization, polymetallic mineralization, and related strata in Xiangshan area (Modified after Guo et al., 2018)

One portion of these compositions is relatively close to those of polymetallic mineralization and metamorphic rock basement, while another portion is closer to those of volcanic rocks. This indicates that, in comparison to polymetallic mineralization, the sources of uranium ore-forming materials are more complex or that the mineralization process was more significantly influenced by contamination from exogenous materials.

5.2 The mineralization model of uranium and polymetallic mineralization

5.2.1 Temporal and spatial relationships of magmatism and mineralization in the Xiangshan area

The age of magmatic and hydrothermal events is important for the understanding of ore deposits from both academic and exploration viewpoints (Stein et al., 1998). Previous studies have concluded that the volcanic activity derived two eruptive circles, forming the main Xiangshan volcanic complex at 135 Ma to 132 Ma (Li et al., 2014; Guo, 2014). Following the extensive volcanic activity,

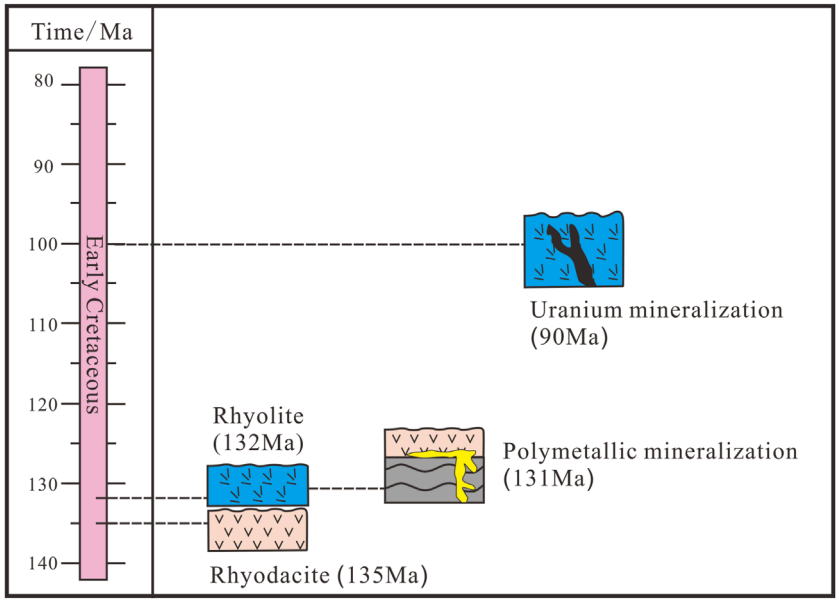

FIGURE 10
Geochronological framework of petrogenesis and mineralization in Xiangshan area. The ages come from Guo et al., 2018; Li et al., 2014, Meng, 2012 and Wang et al. (2023).

the polymetallic mineralization occurred at 131 Ma (Guo et al., 2018). The early Cretaceous was newly discovered and yet to be discovered at the depth of Uranium mineralization. Meng (2012) and Wang et al. (2023) have summarized the ore-forming age of uranium mineralization ranges from 143 to 98 Ma, with a primary focus around 100 Ma. On this basis, we have systematically constructed the geochronological framework of petrogenesis and mineralization in the Xiangshan ore field, as illustrated in Figure 10.

5.2.2 Possible geodynamic setting and genetic model for polymetallic and U mineralization

The geodynamic setting responsible for the Cretaceous magmatism and mineralization has been a controversy. The widespread A-type granites (Chen et al., 2013; Jiang et al., 2011; Peng et al., 2021) and the development of pull-apart basins filled with bimodal volcanic rocks (Li, 2000), such as the Xiangshan volcanic intrusive complex (He et al., 2009; Yang et al., 2010; Yang et al., 2011) strongly suggest that SE China was in an extensional setting during the Cretaceous, mainly caused by the subduction of the Paleo-pacific slab.

Previous studies support a transitional regime from compressive extension at approximately 135 Ma (Mao et al., 2004; Mao et al., 2013), just as it is the time to begin large-scale tectonic-magmatic activities in the Xiangshan area (Figure 11A). During 135–90 Ma, thermal activity related to subduction of the Paleo-pacific slab resulted in the ore fluids and accompanying metals from the enriched lithospheric mantle upwelling (Jiang et al., 2011). The polymetallic ore-forming progress can be divided to two endmembers. One provided the reduced sulfur, and the other provided the important ore-forming metal. The sulfur is mainly derived from mantle reservoirs, gathering and transferring by magmatism. The polymetallic enriched metamorphic basement may have provided the Pb-Sr metals for hydrothermal fluids. Extensive fluid migration and circulation of hydrothermal fluids homogenized isotopically. At about 131 Ma, driven by tectonic and thermal dynamics, the resulting hydrothermal fluids were enriched in metals when migrated upward along regional and local faults and incorporated reduced sulfur-bearing solutions, leading to the precipitation of the polymetallic ores along fracture zones and inter-formational boundaries (Figure 11B). During 100–90 Ma, the polymetallic mineralization process led to continuous enrichment of uranium in deep source regions and changes in physicochemical conditions. The rapid and sustained extension and thinning of the Xiangshan area drove the occurrence of uranium mineralization. Intense crust-mantle material exchange was manifested as an increasingly open uranium mineralization environment. During the uranium mineralization process, abundant crust-derived materials such as country rocks and meteoric water continuously mixed and contaminated the system, resulting in a wide range of sulfur isotopic compositions and lead isotopic distribution patterns similar to those of major geological units in the Xiangshan area (Figure 11C).

6 Conclusion

(1) Comparative analysis of H-O isotopic compositions between uranium and polymetallic mineralization fluids reveals that polymetallic mineralization fluids are primarily derived from magmatic water, whereas uranium mineralization fluids exhibit significant incorporation of meteoric water compared to polymetallic systems.
(2) Comparative study of sulfur isotopic compositions indicates that polymetallic mineralization materials share

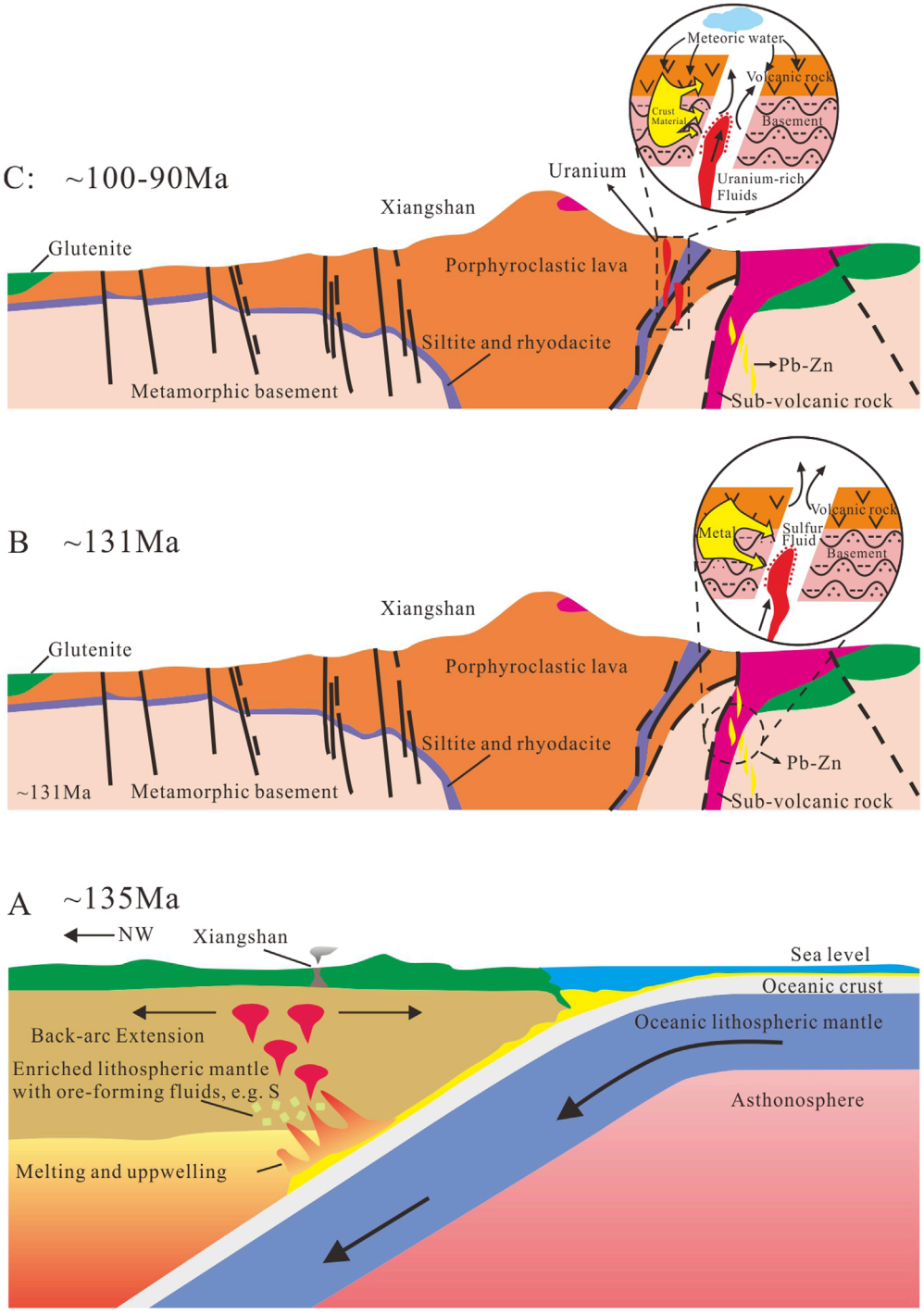

FIGURE 11
(A) Formation stage of Xiangshan volcanic intrusion complex; **(B)** The uranium mineralization stage of Xiangshan ore field; **(C)** The polymetallic mineralization stage of Xiangshan ore field.

consistent sulfur isotopic characteristics with regional typical polymetallic deposits, both originating from magmatic sources. In contrast, sulfur isotopes in uranium mineralization materials suggest substantial contributions from crust-derived materials such as volcanic rocks and basement metamorphic rocks during mineralization.

(3) Lead and strontium isotopic comparisons between uranium and polymetallic mineralization materials demonstrate that uranium mineralization incorporates more crust-derived components (e.g., volcanic rocks and basement metamorphic rocks) compared to polymetallic mineralization. Furthermore, Pb isotopic compositions of polymetallic mineralization

imply potential U-enriched mineralization processes during polymetallic ore formation.

Data availability statement

The datasets presented in this study can be found in online repositories. The names of the repository/repositories and accession number(s) can be found in the article/supplementary material.

Author contributions

JG: Writing – original draft, Writing – review and editing. ZL: Investigation, Writing – review and editing. JN: Investigation, Writing – review and editing. SH: Data curation, Writing – review and editing. JW: Formal Analysis, Writing – review and editing. WK: Methodology, Writing – review and editing.

Funding

The author(s) declare that financial support was received for the research and/or publication of this article. This article is supported by the China Uranium Industry Youth Innovation Fund (YQN2401).

Conflict of interest

The authors declare that the research was conducted in the absence of any commercial or financial relationships that could be construed as a potential conflict of interest.

Generative AI statement

The author(s) declare that no Generative AI was used in the creation of this manuscript.

Publisher's note

All claims expressed in this article are solely those of the authors and do not necessarily represent those of their affiliated organizations, or those of the publisher, the editors and the reviewers. Any product that may be evaluated in this article, or claim that may be made by its manufacturer, is not guaranteed or endorsed by the publisher.

References

Belshaw, N. S., Freedman, P. A., O'nions, R. K., Frank, M., and Guo, Y. (1998). A new variable dispersion double-focusing plasma mass spectrometer with performance illustrated for Pb isotopes. *Int. J. Mass Spectrom.* 181 (1-3), 51–58. doi:10.1016/s1387-3806(98)14150-7

Cannon, R. S., Pierce, A. P., Antweiler, J. C., and Buck, K. L. (1961). The data of lead isotope geology related to problems of ore genesis. *Econ. Geol.* 56 (1), 1–38. doi:10.2113/gsecongeo.56.1.1

Chaussidon, M., and Lorand, J.-P. (1990). Sulphur isotope composition of orogenic spinel lherzolite massifs from Ariege (North-Eastern Pyrenees, France): an ion microprobe study. *Geochimica Cosmochimica Acta* 54 (10), 2835–2846. doi:10.1016/0016-7037(90)90018-g

Chen, K., Gao, S., Wu, Y., Guo, J., Hu, Z., Liu, Y., et al. (2013). 2.6–2.7 Ga crustal growth in Yangtze craton, South China. *Precambrian Res.* 224, 472–490. doi:10.1016/j.precamres.2012.10.017

Fan, H. H., Ling, H. F., Wang, D. Z., Liu, C. S., Shen, W. Z., and Jiang, Y. H. (2003). Study on metallogenic mechanism of Xiangshan uranium ore-field. *Uranium Geol.* 4 (4), 208–213.

Guo, F. S., Yang, Q. K., Meng, X. J., Xie, C. F., Shi, G., Chen, L. Q., et al. (2016). Geochemical characteristics and petrogenesis of the acidic volcanic-intrusive complexes,Xiangshan,Jiangxi. *Acta Geol. Sin.* 90 (4), 769–784.

Guo, J., Li, Z., Nie, J., Huang, Z., Wang, J., and Lai, C. K. (2018). Genesis of Pb–Zn mineralization beneath the Xiangshan uranium orefield, South China: constraints from H–O–S–Pb isotopes and Rb–Sr dating. *Resour. Geol.* 68 (3), 275–286. doi:10.1111/rge.12170

Guo, J. (2014). *The petrology and uranium mineralization alteration study of deep drilling in Xiangshan uranium orefield*. Beijing: Beijing Research Institute of Uranium Geology.

Guo, J., Li, Z. Y., Nie, J. T., Huang, Z. Z., Li, X. Z., Wang, J., et al. (2020). Trace-element geochemistry characteristics of pyrite in polymetallic mineralization in the depth of Xiangshan uranium orefield,Jiangxi Province. *Acta Petrologica Mineralogica* 39 (03), 257–266.

He, G. S., Dai, M. Z., Li, J. F., Cao, S. S., Xia, B., Xu, D. R., et al. (2009). SHRIMP zircon U-Pb dating and its geological implication for the Xiangshan porphyric dacite-rhyolitic. *Geotect. Metallogenia* 33 (2), 299–303. (in Chinese with English abstract). doi:10.16539/j.ddgzyckx.2009.02.007

Jiang, Y. H., Ling, H. F., Jiang, S. Y., Shen, W. Z., Fan, H. H., and Ni, P. (2006). Trace element and Sr-Nd isotope geochemistry of fluorite from the Xiangshan uranium deposit, southeast China. *Econ. Geol.* 101 (8), 1613–1622. doi:10.2113/gsecongeo.101.8.1613

Jiang, Y. H., Zhao, P., Zhou, Q., Liao, S. Y., and Jin, G. D. (2011). Petrogenesis and tectonic implications of Early Cretaceous S-and A-type granites in the northwest of the Gan-Hang rift, SE China. *Lithos* 121 (1-4), 55–73. doi:10.1016/j.lithos.2010.10.001

Kelly, W. C., and Rye, R. O. (1979). Geologic, fluid inclusion, and stable isotope studies of the tin-tungsten deposits of Panasqueira, Portugal. *Econ. Geol.* 74 (8), 1721–1822. doi:10.2113/gsecongeo.74.8.1721

Li, X. H. (2000). Cretaceous magmatism and lithospheric extension in Southeast China. *J. Asian Earth Sci.* 18 (3), 293–305. doi:10.1016/s1367-9120(99)00060-7

Li, Z. Y., Huang, Z. Z., Li, X. Z., Zhang, J. D., Lin, Z. Y., and Zhang, Y. Y. (2014). *Xiangshan igneous rocks and uranium mineralization*. Beijing: Geological Publishing House.

Li, Z. Y., and Zhang, W. L. (2016). Main uranium mineralization types and their comparison of geochemical characteristics in Xiangshan orefield,Jiangxi. *Geoscience* 30 (1), 1–16.

Liu, H. B., Jin, G. S., Han, J., Li, J. J., Zhang, J., and Zhang, J. F. (2015). Metallogenic chronology of hydrothermal uranium deposits in southeastern China. *Acta Geol. Sin.* 89 (S1), 157–159.

Liu, J. L., Li, Z. Y., Nie, J. T., Zhang, W. L., Wang, Y. J., and Tian, M. M. (2019). The timing and ore-forming fluid evolution of deep polymetalic mineralization in western Xiangshan uranium ore field, South China: constraints from Rb-Sr isotope systematics. *Acta Petrol. Sin.* 35 (09), 2787–2800. doi:10.18654/1000-0569/2019.09.11

Mao, J. W., Cheng, Y. B., Chen, M. H., and Franco, P. (2013). Major types and time–space distribution of Mesozoic ore deposits in South China and their geodynamic settings. *Miner. Deposita* 48 (3), 267–294. doi:10.1007/s00126-012-0446-z

Mao, J. W., Xie, G. Q., Li, X. F., Zhang, C. Q., and Mei, Y. X. (2004). Mesozoic large-scale mineralization and multi-stage lithospheric extension in South China. *Earth Sci. Front.* (01), 45–55.

Meng, Y. N. (2012). *Study on the metallogenic mechanism of uranium-thorium ore deposits in the western xiangshan ore field*. Beijing: Beijing Research Institute of Uranium Geology.

Nie, J. T., Li, Z. Y., Wang, J., and Guo, J. (2015). Characteristics of polymetallic ore-forming fluid and metallogenesis of the Xiangshan ore-field in Jiangxi. *Geol. Bull. China* 34 (S1), 535–547.

Peng, H. W., Fan, H. R., Jiang, P., Hu, H. L., and Lan, T. G. (2021). Two-stage rollbacks of the paleo-Pacific plate beneath the Cathaysia block during Cretaceous:

insights from A-type granites and volcanic rocks. *Gondwana Res.* 97, 158–175. doi:10.1016/j.gr.2021.05.020

Rollinson, H. R. (1993). A terrane interpretation of the archaean limpopo belt. *Geol. Mag.* 130 (6), 755–765. doi:10.1017/s001675680002313x

Rollinson, H. R. (2014). *Using geochemical data: evaluation, presentation, interpretation*. London: Routledge.

Si, Z. (2018). "Comparative study on uranium and polymetallic mineralization in Xiangshan ore field,Jiangxi Province,". Master's thesis (Beijing: Beijing Research Institute of Uranium Geology).

Stein, H. J., Sundblad, K., Markey, R. J., Morgan, J. W., and Motuza, G. (1998). Re-Os ages for Archean molybdenite and pyrite, Kuittila-Kivisuo, Finland and Proterozoic molybdenite, Kabeliai, Lithuania: testing the chronometer in a metamorphic and metasomatic setting. *Miner. Deposita* 33, 329–345. doi:10.1007/s001260050153

Sun, Z. X. (2004). Geochemical evidence for uranium sources in Xiangshan uranium ore field. *Acta Mineral. Sin.* 24 (1), 19–24.

Taylor, H. P. (1979). Oxygen and hydrogen isotope relationships in hydrothermal mineral deposits. *Geochem. hydrothermal ore deposits*, 236–277.

Wang, J. G., Chen, R. Q., Xie, G. F., Ji, G. P., and Ma, Y. Y. (2014a). Geological features and prospecting potential of multimetal deposit in Niutoushan area of Xiangshan ore field. *World Nucl. Geosci.* 31 (1), 23–26.

Wang, J., Nie, J. T., and Guo, J. (2015). Characteristic of copper mineralization and fluid evolution in Xiangshan ore field,Jiangxi Province. *J. Mineralogy Petrology* 35 (4), 74–84. doi:10.19719/j.cnki.1001-6872.2015.04.012

Wang, X., Li, S. R., Santosh, M., Gan, H. N., and Sun, W. Y. (2014b). Source characteristics and fluid evolution of the Beiyingxigou Pb–Zn–Ag deposit, central North China Craton: an integrated stable isotope investigation. *Ore Geol. Rev.* 56, 528–540. doi:10.1016/j.oregeorev.2013.02.003

Wang, Y., Fan, H., Qin, K., Evans, N. J., Zhang, C., Zou, X., et al. (2023). Mineralization age of the Xiangshan uranium ore field, South China redefined by hydrothermal apatite U-Pb geochronology. *Ore Geol. Rev.* 160, 105586. doi:10.1016/j.oregeorev.2023.105586

Wu, Z. J., and Hu, Z. H. (2014). Uranium-polymetallic metallogenic characteristics and prospecting direction of Niutoushan uranium deposit in Xiangshan orefield. *World Nucl. Geosci.* 31 (2), 89–94.

Yan, B., Yan, H., Zhou, L., Wang, T., Xu, G. M., and Cao, Y. (2013). Isotopic characteristics of C,O,H,and S in xiangshan uranium orefield,Jiangxi province. *J. Mineralogy Petrology* 33 (3), 47–53. doi:10.19719/j.cnki.1001-6872.2013.03.008

Yang, Q. K., Huang, Q. T., and Sun, Q. Z. (2015). Geological characteristics of sulfer and lead isotopes in the Xiangshan ore field. *Bull. Mineralogy,Petrology Geochem.* 34 (4), 755–762.

Yang, S. Y., Jiang, S. Y., Jiang, Y. H., Zhao, K. D., and Fan, H. H. (2011). Geochemical, zircon U–Pb dating and Sr–Nd–Hf isotopic constraints on the age and petrogenesis of an Early Cretaceous volcanic-intrusive complex at Xiangshan, Southeast China. *Mineralogy Petrology* 101, 21–48. doi:10.1007/s00710-010-0136-4

Yang, S., Jiang, S., Jiang, Y., Zhao, K., and Fan, H. (2010). Zircon U-Pb geochronology, Hf isotopic composition and geological implications of the rhyodacite and rhyodacitic porphyry in the Xiangshan uranium ore field, Jiangxi Province, China. *Sci. China Earth Sci.* 53, 1411–1426. doi:10.1007/s11430-010-4058-0

Yu, X. Q., Wu, G. G., Shu, L. S., Yan, T. Z., Zhang, D., and Di, Y. J. (2006). The cretaceous tectonism if the Gan-Hang tectonic belt, southeastern China. *Earth Sci. Front.* 13 (03), 31–43.

Zartman, R. E., and Doe, B. R. (1981). Plumbotectonics—the model. *Tectonophysics* 75 (1-2), 135–162.

Zeng, Y. J., Li, L., Li, S. R., Santosh, M., Song, Y. X., and Alam, M. (2020). Rb–Sr geochronology and geochemistry of pyrite from the Shihu gold deposit, central North China Craton: implication for the timing and genesis of gold mineralization. *Geol. J.* 55 (8), 5779–5790. doi:10.1002/gj.3543